Atmospheric Ice and Water Content Derived from Parameterization of Nimbus 6 High-Resolution Infrared Sounder Data

ROBERT G. FEDDES[1] AND KUO-NAN LIOU

Department of Meteorology, University of Utah, Salt Lake City 84112

(Manuscript received 18 October 1977, in final form 21 January 1978)

ABSTRACT

A radiative transfer model of spectral infrared radiation in cloudy atmospheres is applied to the most complete set of radiance observations currently available from the Numbis 6 HIRS instrument. The radiative characteristics of clouds in the High-Resolution Infrared Sounder (HIRS) channels are investigated using the discrete-ordinate method for approximating the solution of the radiative transfer equation as it is applied to non-isothermal, inhomogeneous cloudy atmospheres. A method for the estimate of cloud compositions from multi-spectral HIRS radiances, including both shortwave and longwave CO_2 channels, is developed. Theoretical calculations of the upwelling radiance at satellite altitude for a number of thicknesses involving middle level and cirrus clouds are carried out. The resulting theoretical radiances are then parameterized and an empirical method to determine cloud type and ice and water content of the clouds is described. Satellite passes from five days over the western United States are employed to test the empirical parameterizations of the theoretical results. Comparisons of the cloud-type determinations with NOAA 4 mosaic are shown to agree reasonably well. Cloud ice and water content derived from the parameterizations of the HIRS data is compared with that obtained from the Air Force Three Dimensional Neph-analysis (3DNEPH) program. Examples of the application of this technique to global mapping of ice and water content are displayed.

1. Introduction

The newest source of meteorological data in the last decade has come from meteorological satellites. Computer processing of these data has increased the application of satellite data to many long-standing meteorological problems. Each year improved satellite instrumentation becomes available to further enhance the passive remote sensing of the environment. Along with this improved instrumentation are greater volumes of data and the requirement for more computer resources. With these new and improved forms of data, accurate and reliable information can be attained in the inference of the atmospheric state. An important area that is only receiving attention recently is the interpretation of satellite radiance measurements to infer the structure and composition of clouds. This paper describes recent developments on the inference of cloud compositions and structures from a satellite point of view, using some of the most recent data available, and the updated radiative transfer theory applicable to cloudy atmospheres.

The recovery of atmospheric parameters other than clouds has proven to be successful. Accurate atmospheric temperature profiles have been retrieved for clear areas (Chahine, 1970; Smith, 1970). The techniques have also been developed for the determination of the active atmospheric minor gases such as water vapor (see, e.g., Conrath, 1969) and ozone (Prabhakara *et al.*, 1970), and for the estimation of the cloud-top temperature and surface conditions in a clear atmosphere. Furthermore, Smith (1968) and Chahine (1974) have presented a numerical procedure to derive vertical temperature profiles in cloudy atmospheres from two overlapping fields of view. Smith *et al.* (1970) have also treated the cloudy sky problem associated with temperature profile determinations from satellite spectrometer data. Taylor (1974) has further described an approach employing soundings at two different zenith angles to determine temperature profiles in the presence of clouds. However, there has been very little study focusing on the retrieval of cloud properties.

Broad band radiometers such as those on the NOAA and ITOS series of satellites have been used extensively to derive cloud cover in the field-of-view of the satellite radiometer. Many of these methods are completely statistical (see, e.g., Miller and Feddes, 1971). Use of the broadband visible channel to infer cloud thickness from a statistical point of view was done by Park *et al.* (1974) and Kaveney *et al.* (1977) who correlated the low cloud thicknesses directly with brightness observations. The paper by Houghton and Hunt (1971) represents the first attempt to explore the inference of cirrus clouds from passive remote sensing. In conjunction with the possible remote sensing of cirrus cloud composi-

[1] Major, U. S. Air Force, now at Scott Air Force Base, Ill. 62225.

0021-8952/78/0536-0551$08.00

tion, Liou (1974) described emission and transmission properties of cirrus clouds in the 10 μm region. Bunting and Conover (1974) utilized a simple channel-overlapping technique for the estimation of cirrus ice content. Additional research in cirrus clouds was done by Stoffel (1976) in whose work effects of the temperature gradient in the cirrus cloud were considered in the transfer process. Recently, Liou (1977) proposed a retrieval technique for recovering the thickness and ice content of cirrus clouds employing four spectral regions in the 10 μm window.

The purpose of the research described here is to analytically approach the important problem of the interaction of thermal infrared (or terrestrial) radiation with known compositions of cirrus and middle clouds. The formulation of this radiation problem is based on the discrete-ordinate method originally proposed by Chandrasekhar (1950) and further developed by Liou (1973). The method is applied to isothermal layers of model cirrus and middle clouds. The clouds are assumed to be of infinite horizontal extent in a plane parallel atmosphere assumed to be in local thermodynamic equilibrium. The theoretical model is applied to selected HIRS channels with several combinations of middle and cirrus clouds. The theoretical results are parameterized and then used to infer cloud characteristics from actual HIRS data.

Sections 2 and 3 contain a brief description of the characteristics of the HIRS channels and the model atmosphere used in this study and the theoretical considerations for the transfer of spectral infrared radiation through clouds, respectively. Section 4 describes the parameterization of the theoretical results for cloudy atmospheres to infer cloud compositions. Two variables are inferred from this parameterization, and they include the identification of cloud type (cirrus or middle clouds) and the ice and water content of these cloud types. In Section 5, we address the selection criteria for the HIRS data for comparison with 3DNEPH developed at the Air Force Global Weather Central (AFGWC). Finally, we demonstrate the use of the theoretical-empirical parameterizations to indicate the cloud type and equivalent liquid water or ice in cloudy atmospheres, and application of these parameterizations to global mapping of ice and water content from HIRS data.

2. Characteristics of HIRS channels and model atmosphere

The Nimbus 6 HIRS instrument is a third-generation infrared radiation sounder. This instrument is similar to the Infrared Temperature Profile Radiometer (ITPR) on the Nimbus 5 satellite. The instrument scans perpendicular to the satellite subtrack. There are 42 scan spots per scan line with a resolution of 23 km near nadir and 31 km at the extremes of the scan. The Nimbus 6 satellite was successfully launched in June 1975. The HIRS instrument has short periods during which all channels were operating successfully. We have obtained a sample of good data from W. L. Smith (private communication). The data correspond to the period 20–30 August 1975 and cover a geographical area from 80–150°W and 20–50°N. The HIRS instrument senses infrared radiation in 17 channels which include seven channels in the 15 μm CO_2 band, five channels in the 4.3 μm CO_2 band, water vapor channels at 6.8 and 8.6 μm, and three channels in windows at 11, 3.68 and 0.69 μm. In this cloud analysis, only those channels whose peaks of the weighting function are below 100 mb would be substantially affected by clouds. Fig. 1 depicts weighting functions for the HIRS channels. The peak in this figure indicates the approximate location in the troposphere from which its energy is derived.

The model atmosphere used in the theoretical analysis was the mid-latitude summer atmosphere described by McClatchey *et al.* (1972). The model atmosphere was divided in such a way that it would coincide with the pressure levels used in the clear column radiance program (CCR) developed at NOAA/NESS, and supplied to us for our use. There are 40 pressure levels for the CCR program. The program utilizes predetermined transmission profiles which can be adjusted as a function of the atmospheric temperature profile used. To further utilize this predetermined vertical structure and facilitate the execution of the cloud transfer program, the base of the middle cloud was fixed at 700 mb and the top of the high cloud at 250 mb. The thicknesses of the high and middle clouds were allowed to vary from 1.26 to 4.12 km and from 0.35 to 2.68 km, respectively. These values represent realistic thickness variations for high and middle clouds in the atmosphere. Thus two distinct cloud layers with changing thicknesses are formed. The infrared transfer program described below is developed to include all possible combinations of thickness variations. Note that the temperatures of high and middle clouds vary from 244.9 to 270.17 K.

3. The infrared transfer program

The infrared radiation program begins by solving the transfer equation for a plane-parallel cloud layer consisting of cloud particles and absorbing gases in local thermodynamic equilibrium. The basic equation describing the monochromatic infrared radiation field is given by

$$\mu\frac{dI_\nu(\tau,\mu)}{d\tau}=I_\nu(\tau,\mu)-\tfrac{1}{2}\tilde{\omega}_\nu\int_{-1}^{+1}P_\nu(\mu,\mu')I_\nu(\tau,\mu')d\mu' -(1-\tilde{\omega}_\nu)B_\nu[T(\tau)], \quad (1)$$

where I_ν represents the monochromatic radiance of wavenumber ν, μ the cosine of the emergent angle with

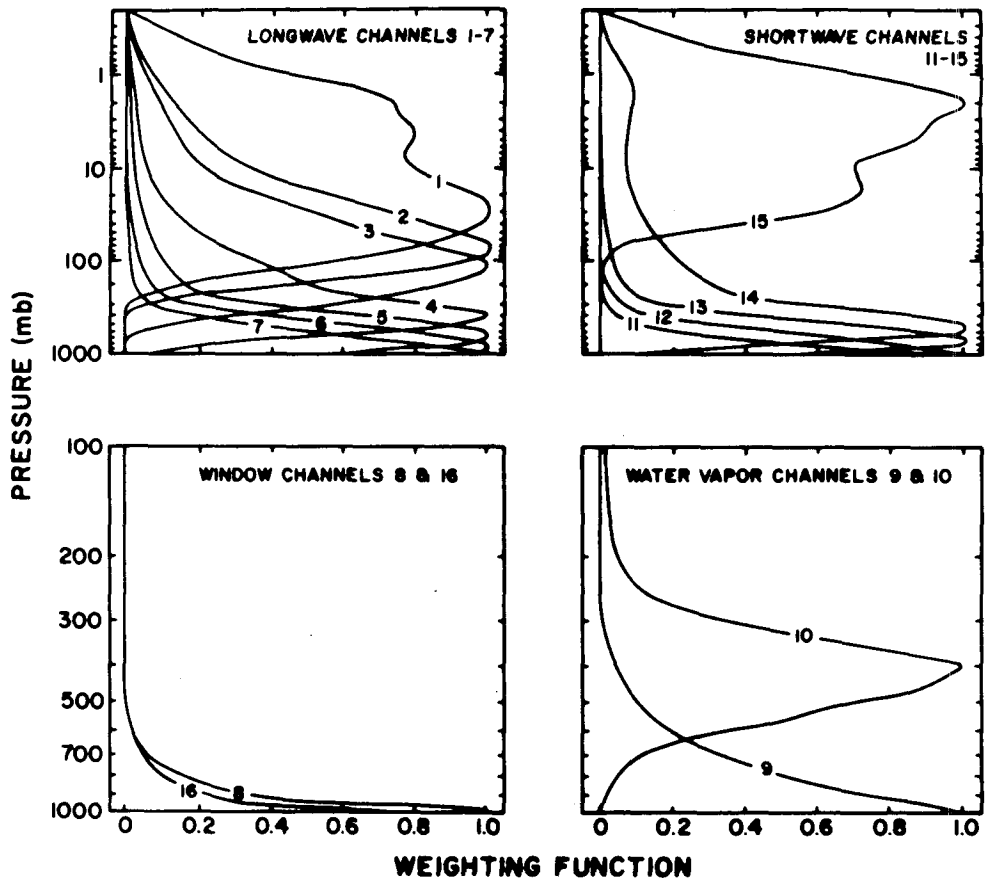

FIG. 1. The weighting functions of the HIRS channels.

respect to the zenith, τ the optical depth, P_ν the normalized axially symmetrical phase function, T the cloud temperature which is a function of height or optical depth, $\tilde{\omega}_\nu$ the single scattering albedo and $B_\nu(T)$ the Planck function.

The normalized phase function may be expanded into Legendre polynomials consisting of a finite number of terms. Upon replacing the integration in Eq. (1) by summation according to the Gauss' quadrature formula, a set of first-order inhomogeneous differential equations can be derived (Chandrasekhar, 1950). The complete solutions of the scattered radiance for a given discrete-stream m assuming an isothermal cloud temperature T_c may be written (Liou, 1974)

$$I_\nu(\tau,\mu_i)=\sum_m L_m\phi_m(\mu_i)e^{-k_m\tau}+B_\nu(T_c), \tag{2}$$

where the summation is taken over the $2m$ ($m=1,2,\ldots$) discrete streams employed, ϕ_m and k_m are the eigenfunction and eigenvalue of the differential equations whose values depend on the phase function and single scattering albedo, and L_m are a set of constants of proportionality to be determined from the radiation boundary conditions above and below the cloud layer.

The spectral upward and downward radiances arising from the molecular absorption and emission reaching the cloud bottom and top, respectively, can be obtained by solving the transfer equation for a nonscattering atmosphere in local thermodynamic equilibrium. Under the assumption that variation of planck function with respect to the wavenumber is much smaller than that of the transmittance, they are given by

$$I_{\Delta\nu}{}^{\downarrow}(z_t,-\mu_i)=\int_{z_t}^{\infty} B_{\Delta\nu}[T(z)]d\tau_{\Delta\nu}(z,z_t;-\mu_i), \tag{3}$$

$$I_{\Delta\nu}{}^{\uparrow}(z_b,\mu_i)=B_{\Delta\nu}(T_s)\tau_{\Delta\nu}(z_b,0;\mu_i)+\int_0^{z_b} B_{\Delta\nu}[T(z)]d\tau_{\Delta\nu}(z_b,z;\mu_i), \tag{4}$$

where $\tau_{\Delta\nu}$ represents the spectral transmittance, T_s is the surface temperature, and z_t and z_b are cloud top and base heights, respectively.

The vertical spectral transmittance for a satellite channel is normally available through the appropriate authority. It may be expressed by

$$\tau_{\Delta\nu}(z)=\tau_{\Delta\nu}(z,\infty;1)=\int_{\Delta\nu}\exp\left[-\int_\infty^z k_\nu(z)n(z)dz\right]\phi(\nu)\frac{d\nu}{\Delta\nu}, \tag{5}$$

where k_ν is the absorption coefficient, n the gaseous number density and $\phi(\nu)$ denotes the instrumental slit function.

Recognizing the definition of the vertical spectral transmittance in Eq (5) it may be approximated by

$$\tau_{\Delta\nu}(\mu) \approx \int_{\Delta\nu} \exp(-\bar{k}_\nu u) \frac{d\nu}{\Delta\nu} \approx \sum_{j=1}^{M} w_j \exp(-k_j u), \quad (6)$$

where u denotes the vertical path length, k_j may be thought of as an equivalent absorption coefficient, w_j is the weight and M denotes the total number of finite terms in the fitting of the transmittances. Note that the infrared spectral transmittance normally cannot be fitted (or approximated) by a single exponential function. Once k_j and w_j have been determined, we may consider the transfer of spectral infrared radiation as monochromatic in the subspectral interval j and carry out transfer calculations in a cloudy atmosphere M times. The upward radiance at the satellite point of view in completely cloudy conditions can now be obtained from

$$I^C_{\Delta\nu}(\infty,\mu_i) \approx \sum_j I^\uparrow_j(z_t;\mu_i)\tau_j(\infty,z_t;\mu_i)w_j + \int_{z_t}^{\infty} B_{\Delta\nu}[T(z)]d\tau_{\Delta\nu}(\infty,z;\mu_i), \quad (7)$$

where $I^\uparrow_j$, the upward radiance at the cloud top, is to be evaluated from the upward and downward radiances arising from the molecular absorption and emission reaching the cloud bottom and top and τ_j is associated with the exponential function given by Eq. (6). Note that $I^\uparrow_j$ cannot be written analytically but is to be computed numerically. The spectral upward radiance at the satellite point of view in clear conditions is simply

$$I^{NC}_{\Delta\nu}(\infty,\mu_i) = B_{\Delta\nu}(T_s)\tau_{\Delta\nu}(\infty,0;\mu_i) + \int_0^{\infty} B_{\Delta\nu}[T(z)]d\tau_{\Delta\nu}(\infty,z;\mu_i). \quad (8)$$

The solution of the infrared radiative transfer equation given by Eq. (2) is applicable only to isothermal and homogeneous cloud layers. To apply the transfer solution to the multilayered cloud system, we divide the cloud layers into a number of sublayers, each of which is considered to be isothermal and homogeneous. By matching the radiation continuity equations for radiances in each sublayer, a set of linear equations with unknown coefficients may be determined by standard matrix inversion methods. A similar procedure has been employed by Liou (1975) to evaluate the transfer of solar radiation in inhomogeneous atmospheres.

The computational procedures begin with the generation of the upper and lower boundary conditions. For this purpose, the CCR program provided by Smith of NOAA/NESS (personal communication) was used. It calculates CCR transmission values at all 40 pressure levels up to 0.1 mb over the range of scan angles of the HIRS instrument. This program was modified to calculate transmittance values at the discrete-ordinate angles used in the radiative transfer program.

The contribution of the absorbing gases within the cloud layer in the transfer calculation were taken into consideration by means of the exponential fitting technique. This fitting utilized the approximation to the vertical transmittance given by Eq. (6). Note here that the amount of water vapor within ice and water clouds is estimated from the saturation condition over ice and water, respectively, whereas the amount of carbon dioxide within the clouds is assumed to be the same as that of the environment.

The single-scattering parameters for altostratus and cirrus cloud were calculated by using scattering computations for the central wavenumber in each band. The cirrus cloud was assumed to be entirely ice and the altostratus cloud was assumed to be all water. Calculation for the ice crystal parameters utilized a theoretical model developed by Liou (1972) which used ice cylinders randomly oriented in a horizontal plane. The major and minor axes of the cylinder used are 200 and 60 μm, respectively, with a concentration of 0.05 cm^{-3}. The single-scattering parameters for the water cloud utilized a drop-size distribution developed by Feddes and Smith (1974). This distribution is an exponential fitting of the best published measurements taken from the cloud physics literature. Although this fitting was done for 10 cloud types, only the altostratus cloud distribution is used. In the calculation of the single scattering parameters for altostratus clouds, a liquid water content of 0.15 g m^{-3} was used. Optical properties of the ice cylinders and water droplets have been presented by Feddes and Liou (1977).

Once the boundary conditions have been generated, the gaseous absorption in the clouds has been fitted and the optical properties of the ice and water have been calculated, the cloud transfer program described previously can now be followed. To obtain the upwelling radiance at the top of the atmosphere, it is necessary to account for the contribution in the atmosphere above the cloud. This step is accomplished by executing the CCR program over a range of satellite scan angles larger than the extremes of the HIRS instrument scan ($\pm 36.9°$). Because only one atmosphere is utilized, this calculation can be made once and for all. The transfer calculation assumes a plane parallel atmosphere. In this case, the scan angle of the satellite is equal to the angle made by the satellite with the local zenith. When viewed from a satellite at scan angles greater than zero, the resolution of the instrument

decreases with increasing scan angle. This decrease in resolution is due to the increase in the distance between the satellite and the sampling point and the curvature of the earth. To account for this difference due to the curvature of the earth, the CCR program uses the angle the earth's local zenith makes with the satellite which is derived from the satellite scan angle. In this way, the contribution to the final upwelling radiance from above the cloud top accounts for the curvature of the earth and as a result, the plane parallel assumption is minimized.

4. Parameterization of radiance calculations from cloudy atmospheres

a. Ratios of upwelling radiances

The theoretical model calculated upwelling radiances for one atmosphere, one cloud temperature and one cloud composition for each cloud type, and over the scan angles of the HIRS instrument. In addition, for computational purposes, the cloud-top height for the cirrus and the cloud base for the middle cloud were held constant. In the real atmosphere, the temperature profile is always changing, the cloud composition is variable, and the location of the clouds in the vertical is never constant. A method that will minimize the effects of the model assumptions when parameterizing the real atmosphere is desirable. The information available from each channel based on the model output is the clear column and cloudy radiances at many scan angles. To minimize the computer requirement and redundancy in the analysis, all the subsequent relationships were derived for a scan angle of 0°. These same relationships could be developed for any scan angle or range of scan angles.

Prior to the empirical parameterization of theoretical results, sensitivity analyses of the cloud thickness on the upwelling radiances for HIRS channels were carried out (Feddes and Liou, 1977). Sensitivity analyses involving cloud thickness were also applicable to cloud particle concentration since the optical depth, which is one of the input parameters in the transfer program, is the linear product of the extinction cross section, the particle concentration and the geometrical thickness. Theoretical sensitivity analyses were done employing the midlatitude summer atmospheric temperature profile because the actual HIRS data that were available were for the period 20–30 August 1975. Variations of the cloud temperature on the upwelling radiance were also examined and some discussions will be given below. Note that the prime purpose of the current investigation has been to develop an empirical technique for the cloud mass inference based on a combination of infrared channels. No attempt has been made to include the cloud temperature or temperature profile inference in this study.

During the course of sensitivity analyses, it was found that the model assumptions for cloudy atmospheres could be minimized by dividing the cloudy radiances by the clear column radiances. This ratio represents the relative reduction of upwelling radiances due to the cloud effects in the atmosphere. There are several advantages in working with these ratios. Physically, the ratio will reduce the effect of the change in atmospheric profile on the cloudy radiances. In addition, the degradation of the ratio coupled with the peaking of the weighting function gives an immediate indication of clouds at that level or above. Another advantage of the ratio technique is that in addition to normalization between different atmospheres, the effects of clouds on the ratio of each channel can be compared with other channels. In the subsequent analysis, channels 4–7 of the 15 μm CO_2 band, 11–14 of the 4.3 μm CO_2 band, 8 at 11.11 μm in the window, 9 in the 8.2 μm water vapor band and 10 in the 6.3 μm water vapor band were utilized.

The theoretical model was executed for cirrus thicknesses of 1, 2, 3 and 4 km and middle cloud thicknesses of 0.3, 0.5, 0.7, 1.0 2.0 and 3.0 km. These ratios are given in Table 1 for cirrus and middle clouds in Parts a and b, respectively. Examination of Table 1 shows that the transparent quality of cirrus is evident in the

TABLE 1. Ratios of cloudy radiances to clear column radiances for 11 HIRS Channels as a function of thicknesses for cirrus clouds (a) and middle clouds (b).

a. Cirrus clouds

Channel	Thickness (km) 1	2	3	4
4	0.970	0.957	0.952	0.950
5	0.866	0.811	0.789	0.780
6	0.799	0.716	0.683	0.670
7	0.748	0.644	0.603	0.587
8	0.743	0.583	0.499	0.452
9	0.718	0.529	0.426	0.371
10	0.960	0.777	0.717	0.697
11	0.538	0.327	0.237	0.200
12	0.563	0.368	0.286	0.253
13	0.679	0.544	0.488	0.465
14	0.858	0.798	0.774	0.764

b. Middle clouds

Channel	Thickness (km) 0.3	0.5	0.7	1	2	3
4	0.996	0.990	0.984	0.979	0.974	0.972
5	0.936	0.921	0.920	0.900	0.889	0.879
6	0.884	0.867	0.865	0.847	0.835	0.835
7	0.839	0.820	0.817	0.804	0.796	0.796
8	0.755	0.720	0.711	0.708	0.708	0.708
9	0.702	0.653	0.641	0.637	0.637	0.637
10	0.997	0.971	0.969	0.968	0.968	0.968
11	0.601	0.519	0.492	0.466	0.453	0.453
12	0.652	0.572	0.549	0.510	0.488	0.488
13	0.813	0.748	0.735	0.668	0.634	0.634
14	0.956	0.919	0.915	0.863	0.863	0.863

infrared spectrum. There is a successive decrease of upwelling radiances in all channels as the cloud thicknesses increase. The successive decrease of the ratios continues all the way to 4 km. Between 3 and 4 km the decrease in ratio in each channel is very slight, indicating that near 4 km the cirrus cloud used in the model is becoming opaque to the infrared radiation, and the cloud temperature now becomes important in the transfer process. At cloud thicknesses greater than 4 km, the upwelling radiance is representative of the Planckian temperature of the cloud top. Analysis of the middle cloud thickness indicates the cloud mass becomes opaque between 2 and 3 km. This can be understood in view of the greater particle concentration when compared to the cirrus cloud.

A decrease of the lower boundary condition in the transfer calculation can be made, in effect by inserting opaque low clouds into the lower atmosphere. The effect on the upwelling radiance as seen from a satellite would be to decrease the ratio. Another decreasing effect would be to use a colder middle cloud temperature. These two cases for middle cloud alone are presented in Table 2 for thick low clouds in Part a and a cloud temperature of 265 K in Part b. Comparison of Table 1b with Table 2a shows some interesting effects on the ratios of the upwelling radiances. The decrease in energy at the middle cloud base due to the presence of opaque low clouds decreases the cloudy to clear column ratio at thicknesses < 2 km, but exhibits the same ratio for thicknesses $\geqslant 2$ km. This again implies that the cloud temperature is the dominant factor in determining the upwelling radiance and thicknesses greater than 2 km. Table 2b represents a calculation with the middle cloud temperature decreased by 5 K from Table 1b and no low clouds present. This table retains the same tendencies as shown in Tables 2a and 1b. The range of the ratios in each channel is decreased when compared to values presented in Table 1b. This decrease in range is caused by the decrease in energy due to the Planckian cloud temperature.

TABLE 2. Ratios for 11 HIRS channel by introducing low clouds (a) and by changing cloud temperature (b).

a. Thick low clouds

Channel	Thickness (km) 0.5	1	2	3
4	0.990	0.979	0.974	0.972
5	0.921	0.900	0.889	0.879
6	0.866	0.847	0.835	0.835
7	0.819	0.804	0.796	0.796
8	0.715	0.708	0.708	0.708
9	0.646	0.637	0.637	0.637
10	0.969	0.968	0.968	0.968
11	0.501	0.465	0.453	0.453
12	0.556	0.506	0.448	0.448
13	0.738	0.668	0.634	0.634
14	0.916	0.863	0.863	0.863

b. Cloud temperature 265 K

Channel	Thickness (km) 0.5	1	2	3
4	0.983	0.975	0.971	0.969
5	0.894	0.878	0.869	0.862
6	0.828	0.812	0.804	0.804
7	0.774	0.760	0.754	0.754
8	0.662	0.647	0.646	0.646
9	0.586	0.566	0.565	0.565
10	0.906	0.899	0.899	0.899
11	0.439	0.387	0.377	0.377
12	0.491	0.435	0.419	0.419
13	0.673	0.612	0.589	0.589
14	0.877	0.838	0.838	0.838

Inner comparisons of the channels in Tables 1 and 2 give a good indication on the effects of clouds on upwelling radiances for different wavenumber regions of the infrared spectrum in conjunction with the peak of the channel's weighting function. The physical factors that influence the ratio for a given cloud type, cloud thickness and channel can be determined from Table 1. Using a 2 km cirrus as an example, the interaction of these two physical factors (the weighting function and the channel wavenumber) are examined. The channels that are in the 15 μm CO_2 band show a decreasing ratio as the weighting functions peak deeper in the atmosphere. The same decrease is noted in 4.3 μm CO_2 channels but by a greater degree. This fact would indicate a greater impact of clouds on shorter wavelengths. The data shows that when comparing channel 7 (peak at 900 mb) and channel 12 (peak at 850 mb) the longwave channel has a ratio double that of the shortwave channel. This effect is probably caused by the wavelength dependence of scattering and absorption properties of cloud particles. Large cloud particles scatter much stronger in the shorter wavelength. The wavelength-dependent scattering effect appears more effective compared to the much higher Planck radiance dependence on temperature at the shorter wavelengths.

This same tendency can be noted for a case of middle cloud only as in Table 1b. Recalling that the middle cloud is based at 700 mb and builds upward. It should be noted that channels with weighting functions that peak above the base of thin middle clouds (4, 5, 10, 14) are not affected by the middle cloud as much as lower peaking channels. Thus, in order to interpret the results of these theoretical calculations, the effects of the cloud temperature, the peak of the weighting function and the wavenumber of the channel must be considered.

b. Cloud-type determination

To utilize the theoretical results in a real atmosphere, the first step to inferring the cloud scene in the satellite

TABLE 3. Slope, y intercept, and correlation coefficient squared for several cloud thickness for cirrus (a) and middle (b) clouds.

a. Cirrus clouds

	Thickness (km)			
	1	2	3	4
Slope	−21.75	−16.82	−14.79	−13.94
y intercept	21.69	15.70	13.68	12.84
r^2	0.872	0.968	0.977	0.977

b. Middle clouds

	Thickness (km)					
	0.3	0.5	0.7	1	2	3
Slope	−22.78	−19.80	−18.80	−18.10	−17.50	−17.50
y intercept	23.56	20.70	19.70	18.80	18.10	18.10
r^2	0.904	0.925	0.925	0.913	0.906	0.906

field-of-view is to determine the vertical location of the cloud. This in effect will give a measure of the cloud type. The foregoing discussions on ratios would indicate the presence of cirrus or middle cloud which can be determined from the analysis of these theoretical results. The presence of middle cloud under a thin cirrus cloud, however, cannot be distinguished from a thick cirrus cloud.

The inability to distinguish multilayer clouds from the current analysis does not hinder the use of this technique to infer cloud thickness. As an example, in the classical warm front, one would expect that by the time a cirrus cloud reaches a thickness of 3 km that middle cloud will be present under this moderately thick cirrus layer. Likewise, with the model indicating a thick middle cloud layer (2 km) lower clouds are probably present. With this in mind, no attempt was made in this analysis to distinguish more than one layer of cloud, although based on thickness calculations and comparisons with satellite pictures, the probability that multilayer clouds exist in the satellite field-of-view is very high.

For the purpose of determining the cloud type from the theoretical data, the channels were rearranged in order of decreasing ratios for a moderately thick cirrus. The rearrangement of the channels from Table 1 is shown in Fig. 2. Analysis of this figure shows the effects of wavenumber and weighting function peak. The longwave channels 4–7 all have greater ratios than the shortwave channels 11–14 with similar weighting function peaks which would indicate that the cloud mass has more impact on shorter wavelengths. The location of channel 14 between channels 5 and 6 would indicate that there is an overlap between the two CO_2 bands depending on the weighting function peak. The locations of channels 10 and 9 are according to weighting function peaks with channel 10 having a higher ratio and a higher weighting function peak than channel 9. The location of their ratios within the CO_2 channel ratios in the figure is due to the model atmosphere humidity profile. By increasing the water vapor amount, there would be an increase in attenuation and thus a lower ratio. Conversely, a decrease in the water vapor would decrease the attenuation and increase the ratio.

The radiance ratios and channel numbers shown in Fig. 2 were each fitted with a linear equation by means of regression analysis. Part a is for cirrus clouds and Part b for middle clouds. Each straight line is labeled with the thickness it represents. The data displayed in Table 1 was fit by a straight line in each case. The equation is of the form $y=a_1R+a_0$, where y is the number assigned to the channel (see Fig. 2) and R the ratio for any given channel and thickness, a_0 and a_1 were derived by standard least-squares-regression procedures and these are related by

$$a_0=\bar{y}-a_1\bar{R}, \tag{9}$$

where

$$\bar{y}=\sum_j y/n, \quad \bar{R}=\sum_j R/n$$

and the summation is for all 11 channels.

Table 3 contains the slope, y intercept, and the square of the correlation coefficient (r^2) for each thickness of cirrus and middle clouds. Analysis of the table shows that the correlation (r^2) is much better in the cirrus case (0.96) when compared to the middle cloud case (0.90). The decrease in correlation in the middle clouds and the 1 km cirrus cases can be explained by the placement of the ratio of channel 10. The original arrangement was done for a thick cirrus case where the effects of the cirrus cloud mass on channel 10 were present. In the middle cloud and 1 km cirrus cases there is no effect of the cloud mass on channel 10. Therefore, the location of channel 10 in the fitting process decreases the correlation for the 1 km cirrus and the middle cloud cases. The linear fit developed here will be used when parameterizing actual HIRS data in the next section. Another important thing to note in this analysis is that the magnitude of the slope is greater than the magnitude of the y intercept for all cirrus thicknesses and the reverse is true for middle clouds. This fact will be used in subsequent analysis to distinguish between middle and cirrus clouds.

Table 2 was also fit with a straight line after rearranging the channels. In both cases, the magnitude of the slope was less than the magnitude of the y intercept which is consistent with earlier middle cloud calculations. Furthermore, both the slopes and y intercepts of Table 4 have smaller magnitudes than those in Table 1. This descrease in slope and y intercept is directly caused by the middle cloud temperature. Since the theoretical calculations indicate that the middle clouds become opaque at a thickness of 2 km, the cloud temperature effects are still present in the ratioing. In the atmosphere, middle clouds generally build from the base up. In the model, the base of the middle cloud was held constant to be consistent. Therefore, a colder cloud

temperature than that used in the model would in effect show an increase in cloud thickness. When this is applied to real data and the slope and y intercept have smaller magnitudes than the ones in the theoretical program, it must be assumed that the cloud is thicker than those that could be handled by the model. Thus, the parameterizations using only one cloud temperature are valid in the present theoretical-empirical study since the presence of a colder cloud temperature would indicate a higher cloud top and therefore a thicker cloud in the model atmosphere employed.

c. Ice and water content determination for the model atmosphere

A measure of liquid water and ice content distribution over the planet is important to many areas of meteorology. These include the initialization of numerical models to increase long-term forecast accuracy and in models that study global circulation and climatic changes. From the theoretical calculations, each cloud thickness is representative of a cloud mass. In the case of water clouds, a liquid water content of 0.15 g m^{-3} was assumed while for ice clouds, a content of 0.0283 g m^{-3} was used.

The recovery of liquid water and ice content from the fitted ratios is possible by knowing the theoretical mass of the cloud for which the ratios are being calculated within certain limits. In the cirrus cloud case, it was found that for a cloud mass of less than 28.3 g m^{-2} the correlation coefficient decreased significantly below the 95% level and the ratios could no longer be fit with a straight line. This was also true for middle clouds with a mass of less than 45 g m^{-2}. Thick middle

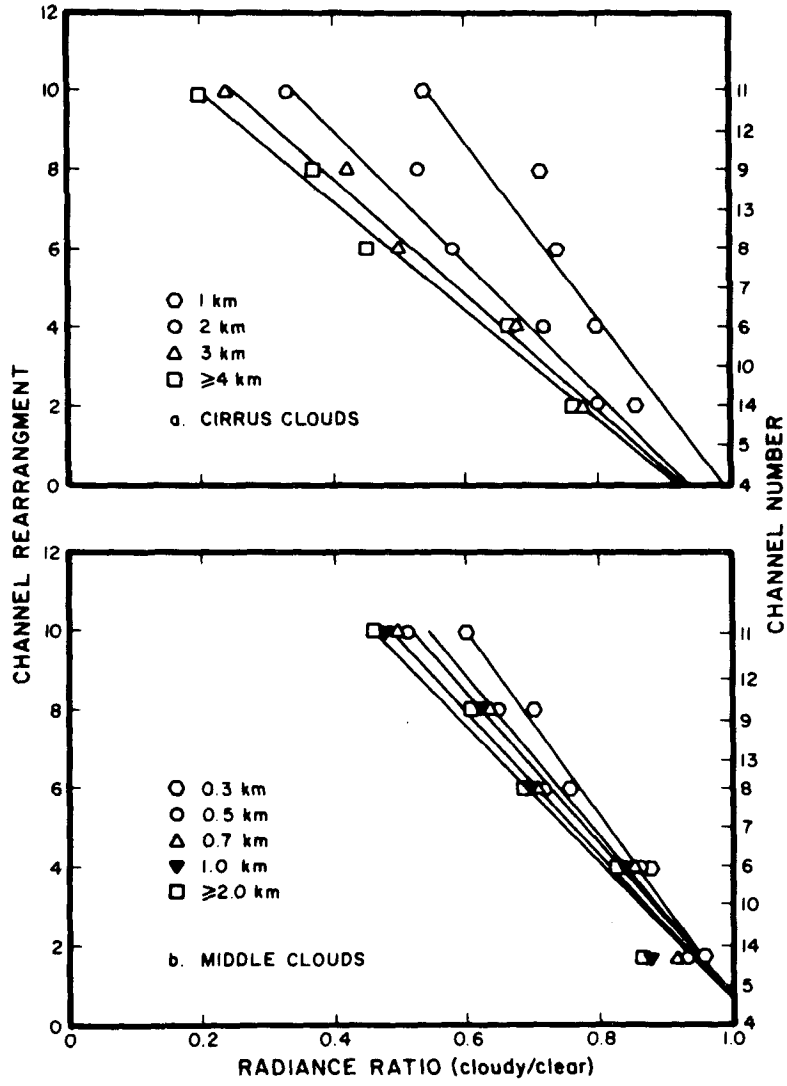

FIG. 2. The best straight line fit for four cirrus cloud thicknesses (a) and for six middle cloud thicknesses (b).

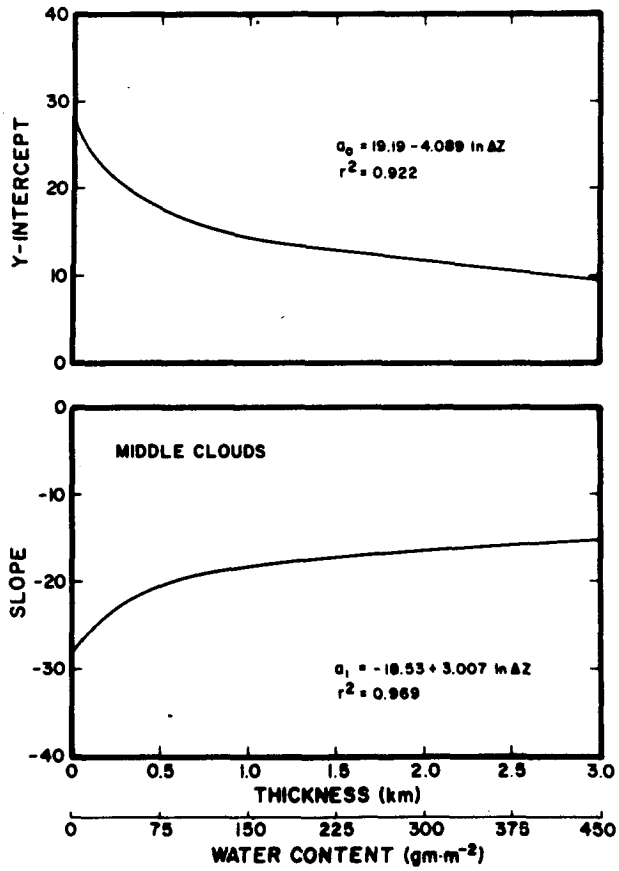

FIG. 3. Best fit of y intercept (top) and slope (bottom) for six middle cloud thicknesses.

clouds (>390 g m^{-2}) had the same ratios as the 300 g m^{-2} (2 km thickness) cloud. This would indicate that the cloud mass is a blackbody and all the energy from below is absorbed by the cloud layer and reradiated. The 113.2 g m^{-2} (4 km thick) cirrus still seems to be somewhat transparent, but this cloud mass was near the maximum that could be handled by the theoretical model.

To recover ice or water content from the parameterizations of the theoretical radiance ratios, the slopes and y intercepts for the two cloud types could be fit by a least-square logarithmic function. It is given for the slope by

$$a_1 = c_1 + c_2 \ln \Delta z \tag{10}$$

and for the y intercept by

$$a_0 = c_3 + c_4 \ln \Delta z, \tag{11}$$

where Δz is the thickness of the ice or water cloud, and c_1, c_2, c_3 and c_4 are constants to be determined for each set of slopes and y intercepts based on the standard least-squares-regression procedures. Six and four cloud thicknesses were used for middle and cirrus clouds, respectively.

Using the data from Table 3, the slopes and y intercepts were fitted for each cloud type. The resulting fits are shown in Fig. 3 for middle clouds and Fig. 4 for cirrus cloud. For middle clouds, c_1 and c_2 are equal to -18.53 and 3.007, respectively, with the correlation coefficient of 0.984, while c_3 and c_4 are equal 19.19 and -4.089 with a correlation coefficient of 0.960. For the cirrus case, the values of c_1, c_2, c_3 and c_4 are -21.40, 5.75, 21.19 and -6.526, respectively. The constants c_1 and c_2 had a correlation coefficient of 0.988, while c_3 and c_4 had a correlation of 0.983.

Upon substituting a_1 and a_2 in Eqs. (10) and (11) into Eq. (9), the thickness of any middle or high cloud is given by

$$\Delta z = \exp[(\bar{y} - \bar{R}c_1 - c_3)/(c_2\bar{R} + c_4)]. \tag{12}$$

The cloud mass is then derived by multiplying the cloud thickness in kilometers by 28.3 g m^{-2} km^{-1} for cirrus cloud and 1.5×10^2 g m^{-2} km^{-1} for middle clouds.

5. Data description and selection

The method to determine cloud type and ice or water content developed in the previous section was applied to a selected set of Nimbus 6 HIRS data. The results

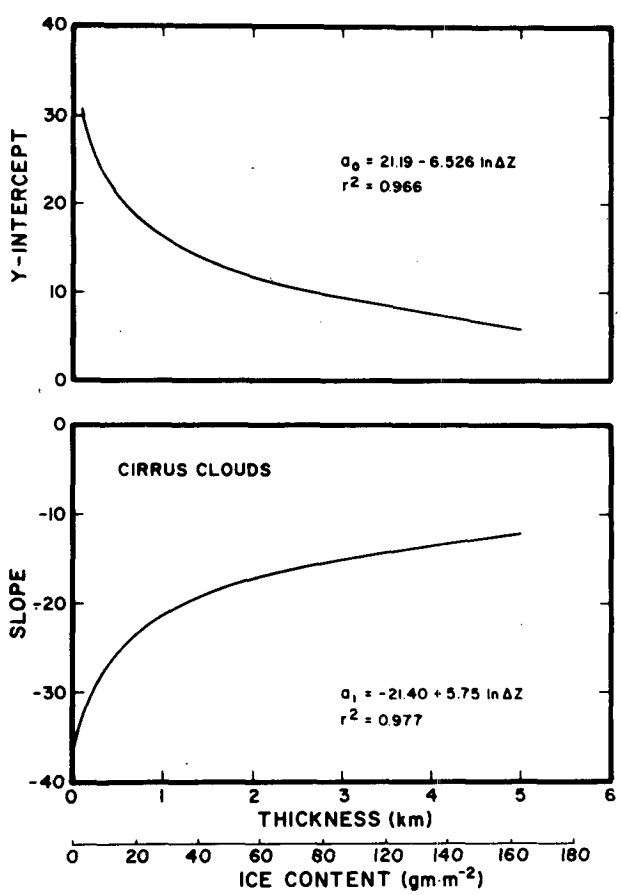

FIG. 4. Best fit of y intercept (top) and slope (bottom) for four cirrus cloud thicknesses.

of this application were compared to the 3DNEPH and satellite cloud pictures since these were the only source of consistent cloud information on a routine basis. In this section, the HIRS data used in this analysis and the 3DNEPH data base are described.

a. The three-dimensional nephanalysis data

The 3DNEPH program was developed at the AFGWC to incorporate the tremendous quantity of satellite-sensed cloud data and conventionally sensed meteorological parameters into a three-dimensional cloud model of the atmosphere. Basic to the design of the 3DNEPH is the assumption that satellite information is available for its data base in a timely manner. However, in the event that satellite data are not available, the 3DNEPH has the capability of extrapolating past analysis until such time as satellite data do become available.

The 3DNEPH program is built as a series of input processors. These processors include the surface data processor, radiosonde observation (RAOB) processor, aircraft data processor, manual data processor, decision tree processor, satellite video data processor, satellite infrared data processor, final processor, forecast processor, verification processor and display processor. Because of the modular nature of the 3DNEPH program, processors can be added to or deleted from the system with a minimum of programming problems. Descriptions and functions of each of the processors can be found in the AFGWC Technical Memorandum 71-2 (Coburn, 1971).

The hemispheric grid chosen for the 3DNEPH, which was compatible with the accuracy of its input satellite data, was a 512×512 array centered at the north (south) pole of a polar stereographic map and having a distance between grid points of 40 km at 60° latitude. This 512×512 grid was further subdivided into 64 squares (boxes), so that the finest mesh was 4096 grid points over each hemisphere. The vertical resolution of the 3DNEPH program divides the atmosphere into 15 layers. In addition to the information given for cloud amounts in the layers, seven pieces of data are given at each point that pertain to the point. These data denote information about the cloud types, maximum tops and minimum bases, the current weather and the total cloud cover.

The 3DNEPH was used as a comparison since no other known source containing the routine analysis of cloud parameters is available. The use of the 3DNEPH as a source of comparison to the techniques developed here has many shortcomings. These problems include timeliness, layer resolution, dependence on subjective observations and the horizontal spreading of the data.

The timeliness of data is very crucial in this analysis. The 3DNDPH is produced every 3h. If there are no new data for an update, the previous analysis or a cloud forecast is used for the new analysis. The ever-changing cloud scene at a point makes the timeliness of the 3DNEPH and the HIRS data very important. This problem is minimized since we are considering overcast cases in which the cloud scene at a point will probably not change significantly over a short period of time.

A second problem area is the layer resolution of the 3DNEPH. In middle cloud layers this can be as much as one layer thickness, i.e., up to 4000 ft. In the high cloud layers this can be up to 20 000 ft. If a thin layer of cloud is reported to be in one of the layers, the model must automatically fill the entire layer with clouds. As noted earlier, an error of 4000 ft (1.2 km) is one-half the thickness of middle cloud that can be detected by the theoretical model. In the case of cirrus clouds, a 20 000 ft error is equivalent to 6.1 km, a greater thickness than the model can handle. This large error can be somewhat offset when the maximum cloud-top parameter is considered. At middle and high cloud-top levels, the coding for this parameter is accurate to 5000 ft or 1.5 km. For lower middle cloud tops, this parameter is accurate to 1000 ft or 0.3 km.

The use of subjective weather observations plays an important role in the accuracy of the 3DNEPH clouds. If there are no current satellite data, the cloud top cannot be determined and persistence prevails. The cloud thickness would be overestimated or underestimated. Another case would be when satellite data are available but no surface observation is present (over oceans); in this case the satellite can estimate the cloud-top height only and no information about the cloud depth can be determined. For optically thin cloud, the satellite data used in 3DNEPH program underestimates the cloud height.

The need to take surface observations and spread them horizontally is another area in which the comparison would not match. The 3DNEPH grid point represents a 40 km box at 60°N. If there are no current satellite data and the observation network is not at a 40 km resolution, some influence of the surface observation is spread to adjacent points in the 3DNEPH. This can be seen by examining an area of 3DNEPH data where the cloud thickness will be constant over a large area. Steps taken to minimize these problem areas will be discussed below.

b. High-resolution infrared sounder data

The data that are routinely processed at NOAA/NESS are available on nine-track, 1600 bpi tapes. The data are packed in such a way that six or seven orbits are available on each tape. These tapes contain located and calibrated radiance values for all 17 channels. The *Nimbus 6 User's Guide* (Smith *et al.*, 1975) gives a detailed explanation of the calibration procedure used on the radiance measurements in each channel. The resolution of the HIRS data decreases

with increasing scan angle. This decrease in resolution of a scan spot is from approximately 23 km at nadir to 31 km at a scan angle of 36.9° as noted previously in Section 2.

The data set used in this analysis was for 20–30 August 1975, a time when all channels of the HIRS instrument were operating properly. Further, it was required to have data over North America since the comparison was being used with the 3DNEPH which depends heavily on good surface observations. We therefore requested data from 20–55°N and 80–105°W which includes both land and ocean areas. To further complicate the data selection, examination of satellite photographs indicated a general lack of middle and high clouds over this region except areas north of 40°N for this time period. As a result, all of the data cases used in the analysis are along the storm track north of 40°N. The data that we had were not corrected for the solar radiation contamination in the shortwave channels. The reflected sunlight has a pronounced effect in channel 16, the shortwave window, which, however, was not used in the present analyses.

A total of 26 passes were provided in the data set of which five were analyzed for cloud information at the two scan angles closest to nadir. To check consistency of the data from channel to channel within a pass, the five passes used in the analysis were displayed by using an overprinting technique to simulate grey shading on the line printer. All the passes used in subsequent analyses were overprinted to verify the HIRS data by comparing the overprints with surface analysis and NOAA satellite visible and infrared mosaic.

The basic criteria for the selection of the HIRS data to be compared with the 3DNEPH must consider the use of data where the 3DNEPH is most reliable. This criteria dictated that data be chosen where the 3DNEPH had good surface data as well as satellite data. Additionally, the areas of interest must be in the presence of synoptic-scale weather so that continuous cloud decks would be insured. The use of HIRS data points at or near nadir would insure the least amount of error in applying the real data to the theoretical calculations, since the fitting of the theoretical upwelling radiances to different scan angles would be most accurate at nadir.

Based on the foregoing criteria, five passes on five consecutive days were chosen for this comparison. These days included 21–25 August 1975. The pass on each day that included western North America and is closest to a 3DNEPH analysis time is used. Since Nimbus 6 has an approximate equator crossing at 1200 local time on its ascending pass, this would correspond to 1800 GMT analysis time for the 3DNEPH. The area of the 3DNEPH that covers this area in box number 44 which has the following latitudes and longitudes for the upper left, upper right, lower left and lower right, respectively: 52°N, 125°W; 62°N, 80°W; 31°N, 106°W; and 36°N, 80°W. Inspection of satellite pictures on these five days shows that all the clouds are north of 40°W and a majority of them are north of 45°N. For this reason, all the points used in the comparison are at these latitudes.

To apply the theoretical results to the real HIRS data, which is for midlatitude summer, a method had to be developed to reduce the cloudy radiances to ratios. The theoretical data would be compatible since the atmosphere used in the calculations was midlatitude summer. To obtain a clear column radiance that is representative of a localized area, the HIRS data were examined in conjunction with the satellite pictures. The point chosen for the clear column radiance, which had the same scan angle as the cloudy radiances, was then used to obtain the cloudy ratios for that day. This choosing was done for all five days to obtain ratios for the cloudy cases.

The colocation of the HIRS data with the 3DNEPH was accomplished using the latitude and longitude from the HIRS data. These quantities were then converted to 3DNEPH grid location. Since this location is never an exact 3DNEPH point, the 3DNEPH point used for the comparison was that point closest to the calculated grid location.

6. Cloud type and mass determination from HIRS data

a. Cloud type

All of the HIRS data applied to the theoretically based empirical relationships are from the cloudy areas north of 40°N. The slope and y intercept of each case was calculated. The cases with the magnitude of the slope greater than the magnitude of the y intercept were assumed to be cirrus clouds. The cases with the magnitude of the y intercept greater than the magnitude of the slope were assumed to be middle or lower clouds. These cases were then examined in conjunction with the IR pictures. In all cases, the empirically derived relationships that were based on the theoretical model indicated the proper cloud type.

The theoretical empirical model indicated the presence of middle clouds in the vicinity of 52°N, 115°W to 43°N, 100°W on 21 August. Examination of the IR picture not shown here verifies the presence of lower clouds in this area. For 22 August, the model indicated a mixture of cirrus and lower clouds from 52°N, 104°W to 49°N, 102°W and then extensive lower clouds to 43°N, 99°W. This same pattern can be noted by examining Fig. 5. In the vicinity of 50°N the IR picture shows an area of some cirrus clouds and some warmer lower clouds. South of 49°N there are only lower clouds in the IR picture of Fig. 5. It also indicates little cloud south of 43°N. One of the clear points in this area was used for the clear column

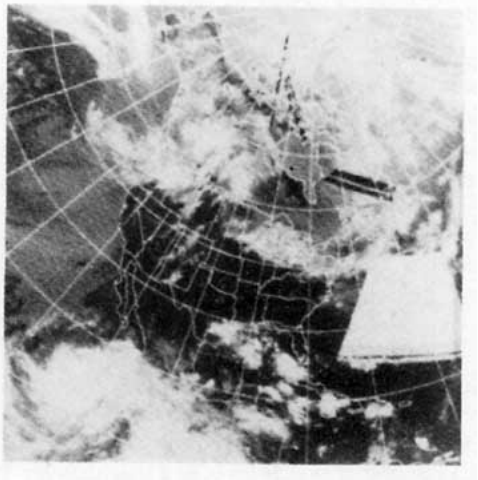

FIG. 5. NOAA 4 infrared picture for 22 August 1975.

radiance in the ratioing for this day. The IR picture for 23 August (not shown here) indicates extensive cirrus on the subtrack of the satellite from 53°N, 120°W to 42°N, 115°W. The model shows all cirrus clouds in this area except for the indication of some middle clouds near 53°N. Further examination of the IR picture on this day reveals some breaks in the cirrus cloud in this area. On 24 August, cirrus was again indicated from 52°N, 109°W to 48°N, 106°W and middle clouds were present south of 47°N. Examination of the satellite picture for that day not shown here verifies this analysis. The clear column radiance for this day was taken from an area just south of 47°N along the subtrack of the satellite. The model analyzed middle clouds from 53°N, 97.5°W to 47°N, 94.5°W and cirrus clouds from 44°N, 93°W to 39°N, 91.7°W for 25 August. This again is represented well on the IR picture of Fig. 6. The clear column radiance for this day was from near 38°N, 91°W. The ice and liquid water content for this pass along with the pass for 22 August are mapped in a subsequent section.

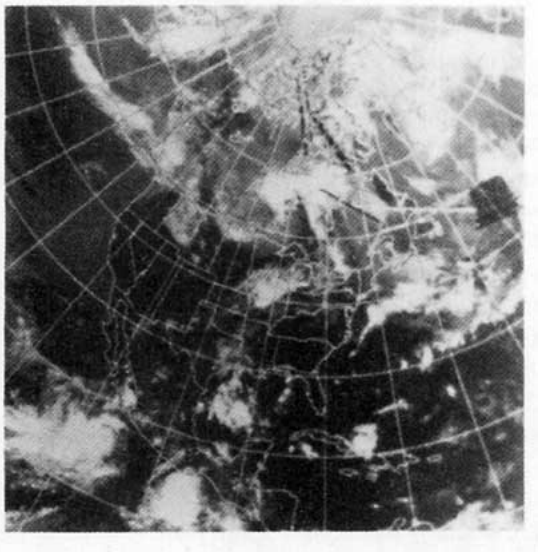

FIG. 6. As in Fig. 5 except for 25 August 1975.

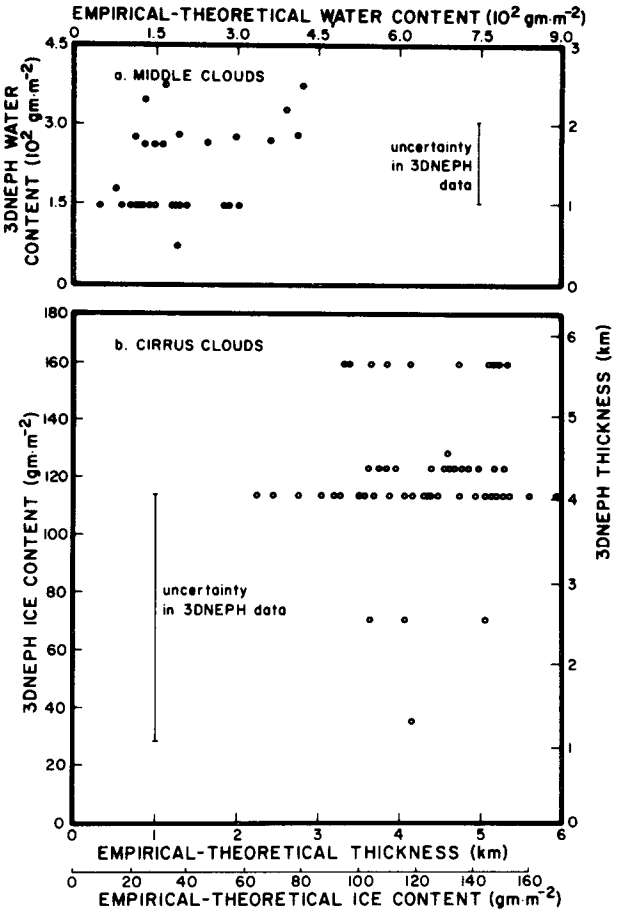

FIG. 7. Comparison of 3DNEPH middle cloud water content with empirical-theoretical middle cloud water content from HIRS (a) and comparison of 3DNEPH cirrus cloud ice content with empirical-theoretical cirrus ice content from HIRS (b).

b. Cloud mass

To determine the cloud mass thickness and mass, the data described in the previous section were divided into middle and high clouds. Note that the cloud thickness was derived from Eq. (12) utilizing the HIRS data. The 3DNEPH points that correspond to these data cases were then selected from Box 44 of the 3DNEPH at 1800Z for the five days analyzed. In all cases, the 3DNEPH indicated lower clouds below the cirrus or middle cloud. This indicates one of the basic problems discussed earlier about the 3DNEPH, that with only surface analysis, the cloud top is overestimated, whereas with only satellite data, the cloud base is lower than it should be. Thus, the error can be greater than the thickness of the cloud. It is virtually impossible to correct this problem without instrumentation that can see through clouds. In addition, the spreading of an observation to many

3DNEPH points tends to smooth the area out so that cloud thicknesses are constant over large areas. To minimize these problems, the 3DNEPH cloud thickness data were used as either cirrus or middle cloud. As noted earlier, this would not affect the ice and water content calculation significantly because middle cloud in the presence of thin cirrus has the same appearance as moderately thick cirrus. The effect of lower clouds on middle cloud ratios remained virtually unchanged when comparing the slopes and y intercepts derived from the empirical-theoretical approach.

Fig. 7 is a graph comparing the model ice and liquid water contents with the 3DNEPH derived ice and water contents. Parts a and b of the graph are for middle and cirrus cloud cases, respectively. In both parts, both the 3DNEPH and the theoretical-empirical relationships indicated middle or cirrus clouds. Comparison of the 3DNEPH derived water contents in Fig. 7a with the empirically derived theoretical water contents are somewhat variable. The linear relationship desired is not present although some correlation can be noted. The data points in the comparison primarily occur at four 3DNEPH middle cloud thicknesses in its data base while the model-derived water contents cover a wide range. The error range of the comparisons for Fig. 7a is up to 2.25×10^2 g m^{-2}. Analysis of Fig. 7b also indicates the grouping of the 3DNEPH data at basically three ice content values although the range from the empirical–theoretical calculations vary over a wide range for a given 3DNEPH value. The error range in Fig. 7b is up to 84.9 g m^{-2}. Although the desired linear result is not present for the comparisons in Fig. 7, some agreement between the two different methods of computing cloud ice or liquid water content is indicated. It should be noted that the two methods are not totally independent since the 3DNEPH data also contain Air Force infrared data.

The above comparisons point out the simple fact that new methods for determining cloud structures from satellite data cannot be properly verified with the current data bases that are available. The cloud typing derived in this analysis can be compared with simultaneous cloud photographs and these comparisons appear to be good in light of discussions in the previous section. The verification of ice and liquid water content will require well planned and controlled measurements of cloud structures within the satellite field-of-view. With this type of verification, it will be possible to reformulate parameterizations of theoretical calculations to improve the accuracy of these estimates of cloud compositions. Until this can be accomplished, the use of theoretical-empirical relationships should prove to be more accurate than purely statistical methods.

c. Cloud moisture mapping

The use of the parameterizations described in the previous section and applied to HIRS data in this section can be used to map ice and water content of middle and cirrus clouds. To perform this mapping on a global scale over long periods of time would be the desired result. However, to accomplish this on a routine basis would require the availability of global satellite data and a large block of dedicated computer time. In this section portions of two orbits over central North America are mapped to illustrate the concept.

The map used for these projections is polar stereographic and it is therefore possible to make comparisons easily with NOAA 4 satellite pictures. In each of the cases the clear column radiance at satellite nadir was used to perform the ratioing over 10 scan spots on each side of the nadir. Beyond these scan angles, a clear column radiance representative of a large scan angle should be used to perform the ratioing to derive the amount of liquid water or ice content.

As noted earlier, the slope and y intercept of the linear fit determine whether middle or high clouds are present. If the magnitude of the slope is greater than the y intercept, cirrus cloud is assumed. Further criteria established to perform the mapping were to eliminate data points where the magnitude of the slope is greater than 25, or the correlation coefficient was less than 0.70. These criteria were used after comparing many cases of actual data with theoretical calculations. Cases that do not meet the above criteria are low cloud which were not addressed in this analysis.

In both passes analyzed, the latitudes and longitudes of the data points that met the above criteria were plotted on the polar projection and then analyzed. The two figures (Figs. 8 and 9) containing the analysis are for 22 and 25 August, respectively. In both cases, the cirrus and middle cloud are mapped on the same figure.

The analysis for 22 August shows two areas of overcast conditions under the satellite. The northern area is over southern Canada and extreme northern Montana and North Dakota, and is characterized by both middle and high clouds. Since the data is cutoff to the north, east and west, the analysis shows sharp break points in these directions. Analysis of the NOAA 4 pictures indicates that little cirrus cloud is present in the southern cloud areas analyzed for this pass, in agreement with the present analysis. The theoretical analysis also shows middle cloud less than 1 km thick both south of the northern area and north of the southern area of clouds.

Analysis of the figure for 25 August shows a similar set of two distinct cloud areas. The southern area is the cirrus on top of an active area of thunderstorms and the sharp southern edge of this cloud mass corresponds very well to the NOAA 4 picture. The

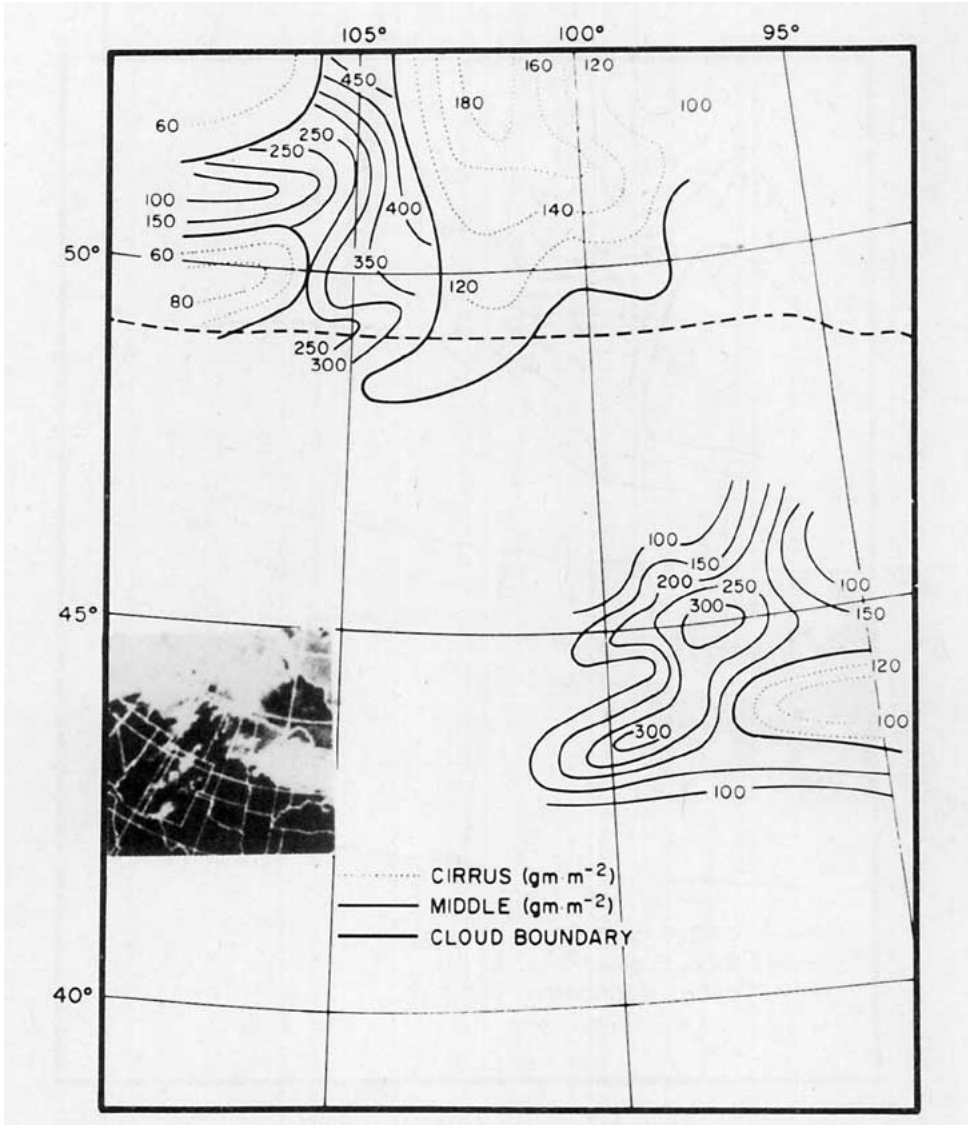

FIG. 8. Cloud ice and water content based on empirical-theoretical calculations for 22 August 1975. Dotted lines are for cirrus clouds (g m^{-2}) and solid lines for middle clouds (g m^{-2}). Heavy lines are the cloud boundaries.

northern cloud mass is dominated by middle cloud with some cirrus on the southwest side. This again agrees well with the NOAA 4 satellite picture. On the southern edge of the northerly cloud mass the middle cloud thicknesses fall off very rapidly both by examination of the picture and from mapping.

The current analysis seems to lend itself to real-time analysis because the computer time requirement has been minimized by the empirical parameterizations. In addition, the ratioing has decreased the effect of the real atmosphere on the cloud liquid water and ice content determination. No claim is made, however, that the present technique for ice and water content determination in midlatitude summer condition can be extended to other atmospheric profiles.

When compared to microwave techniques the technique developed here has both advantages and disadvantages. Two advantages are the higher resolution of the HIRS instrument when compared to the Nimbus 6 Scanning Microwave Spectrometer (SCAMS) instrument and the detection of cirrus clouds that are transparent in the microwave portion of the spectrum. Another advantage of this technique is that it can be applied over both land and oceans, while microwave interpretation of clouds is restricted to oceans because of the change of land emissivity. Disadvantages of this technique when compared to microwave includes the opacity of water clouds in the infrared portion of the spectrum and the sensitivity of the technique to the water cloud temperature. By combining infrared and microwave measurements along with the proper

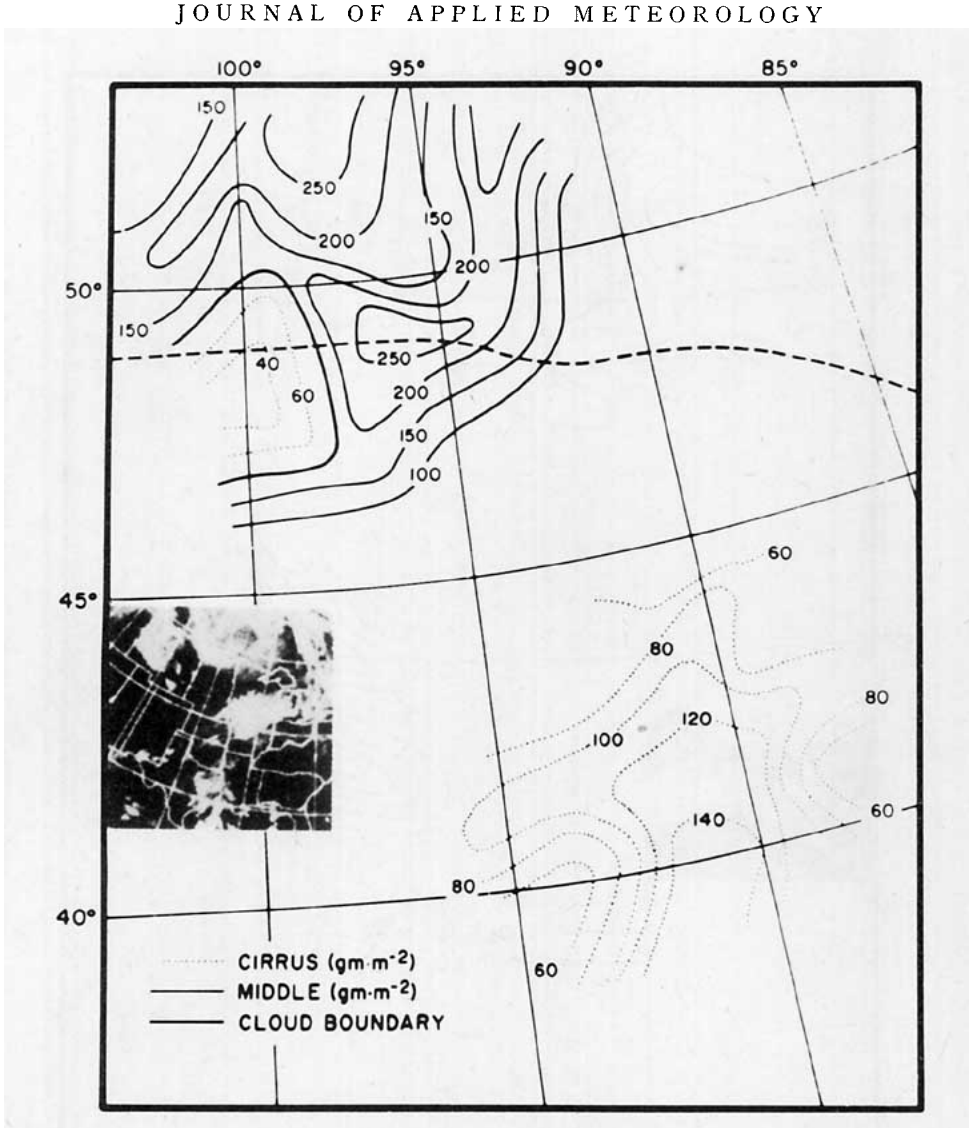

FIG. 9. As in Fig. 8 except 25 August 1975.

cloud physics verification data, operationally significant recovery of cloud parameters from satellite data appears feasible.

7. Conclusions

A theoretical model that calculates transfer of spectral infrared radiation based on the discrete-ordinate method was developed to include cirrus and middle clouds and absorbing gases. This analysis used one model atmosphere and one middle and high cloud type for all calculations. The top of the cirrus cloud and the base of the middle cloud were held constant to minimize computer time. The layers in the transfer computations were assumed to have constant temperatures so that the effects of the change in cloud thickness on the upwelling radiance could be studied. Various thicknesses and combinations of middle and cirrus clouds were used in the analysis. This model was then applied to the HIRS channels of the Nimbus 6 satellite. Available transmittances for each of the channels used were employed and modified to generate upper and lower boundary conditions and gaseous absorption in and between the cloud layers.

The theoretical calculations of upwelling radiance were divided by their clear column radiances to give a ratio for each channel. These ratios were then fitted with a straight line for each theoretical cloud thickness for both cirrus and middle clouds. It was found that cases where the slope was greater than the magnitude of the y intercept derived from transfer calculations corresponded to cirrus clouds. The reverse of the slope and y intercept relation corresponded to middle clouds or lower clouds. The resulting slopes and y intercepts for different cloud thicknesses for the two cloud types were then fitted with a logarithmic function. This made it possible to infer ice and water content in the case of high and middle clouds, respectively, for a given thickness based on the theoretical calculations.

These theoretical parameterizations were applied to five days of HIRS data. The empirical parameteriza-

tion method appears to be successful in identifying high and middle clouds. The resulting cloud ice and liquid water contents were then compared to the 3DNEPH to indicate whether this technique could be applied in an operational mode. It was found that the comparisons with the 3DNEPH were marginal. This can be traced to the 3DNEPH and the methods used to determine cloud thicknesses as well as approximations in the theoretical calculations and the parameterization of these calculations. Two days of ice and water content for actual HIRS data were then mapped. These results were good when comparing the resulting maps with the corresponding NOAA 4 infrared and visible satellite pictures.

The technique developed in this paper is ideally suited to enhance the cloud parameterizations in the 3DNEPH. As noted earlier the 3DNEPH is a modular program that processes all kinds of meteorological data. The only currently used satellite data are broadband visible and infrared channels of a NOAA 4 type scanning radiometer. The addition of this technique would use satellite data that are not in current use for cloud detection and it would give valuable input into the final results. Since the 3DNEPH is a routinely produced product, much of the software required to implement this procedure is already in existence and the operational development could be carried out independently of 3DNEPH production. As noted earlier the resolution of the HIRS and the 3DNEPH are similar so that in an operation implementation the 3DNEPH could be used to further verify the technique.

Further studies seem warranted for the determination of cloud parameters from satellites. Although an objective way of deriving cloud type information and cloud ice or water content has been illustrated in this analysis, a more reliable method of verification must be found. However, verification of satellite sensing techniques requires carefully designed field experiments in which highly reliable cloud parameters could be obtained under the satellite pass. With sufficient cases from which cloud parameters may be derived locally, intercomparisons with satellite derived values may be carried out to establish the statistical significance of this technique to parameterize satellite measurements.

Acknowledgments. This research was supported by the Air Force Geophysics Laboratory under Contract F19628-75-C-0107. We thank Dr. W. Smith for providing us with the HIRS data utilized in this investigation.

REFERENCES

Bunting, J. R., and J. H. Conover, 1974: Estimates from satellites of total ice and water content of clouds. *Preprints Int. Conf. Cloud Phys.*, Boulder, Amer. Meteor. Soc., 407–412.

Chahine, M. T., 1970: Inverse problems in radiative transfer: Determination of atmospheric parameters. *J. Atmos. Sci.*, **27**, 960–967.

——, 1974: Remote sounding of cloudy atmospheres. I. The single cloud layer. *J. Atmos. Sci.*, **31**, 233–243.

Chandrasekhar, S., 1950: *Radiative Transfer.* Dover, 393 pp.

Coburn, A. R., 1971: Improved three-dimensional nephanalysis model. Air Force Global Weather Center Tech. Memo. AFGWCTM 71-2, 72 pp.

Conrath, B. J., 1969: On the estimation of relative humidity profile from medium resolution infrared spectra obtained from a satellite. *J. Geophys. Res.*, **74**, 3347–3361.

Feddes, R. G., and R. D. Smith, 1974: A synoptic scale model for simulating condensed atmospheric moisture. USAFETAC TN74-4, U. S. Air Force Environmental Technical Applications Center, Washington, D.C., 31 pp.

——, and K. N. Liou, 1977: Sensitivity of upwelling radiance in Nimbus 6 HIRS channels to multilayered clouds. *J. Geophys. Res.*, **82**, 5977–5989.

Houghton, J. T., and G. E. Hunt, 1971: The detection of ice clouds from remote measurements of their emission in the far infrared. *Quart. J. Roy. Meteor. Soc.*, **96**, 1–17.

Kaveney, W. J., R. G. Feddes and K. N. Liou, 1977: Statistical inference of cloud thickness from NOAA IV scanning radiometer data. *Mon. Wea. Rev.*, **105**, 99–107.

Liou, K. N., 1972: Light scattering by ice clouds in the visible and infrared: A theoretical study. *J. Atmos. Sci.*, **29**, 524–536.

——, 1973: A numerical experiment on Chandrasekhar's discrete-ordinate method for radiative transfer: Applications to cloudy and hazy atmospheres. *J. Atmos. Sci.*, **30**, 1303–1326.

——, 1974: On the radiative properties of cirrus in the window region and their influence on remote sensing of the atmosphere. *J. Atmos. Sci.*, **31**, 522–532.

——, 1975: Applications of the discrete-ordinate method for radiative transfer to inhomogeneous aerosol atmospheres. *J. Geophys. Res.*, **80**, 3434–3440.

——, 1977: Remote sensing of the thickness and composition of cirrus clouds from satellites. *J. Appl. Meteor.*, **16**, 91–99.

McClatchey, R. A., R. W. Fenn, J. E. Selby, F. E. Volz and J. S. Garing, 1972: *Optical Properties of the Atmosphere*, 3rd ed. AFCRL-72-0497.

Miller, D. B., and R. G. Feddes, 1971: Global atlas of relative cloud cover 1967–1970 based on data from operational satellites. National Environmental Satellite Service, Washington, D.C., 237 pp.

Park, S. U., D. N. Sidkar and V. E. Suomi, 1974: Correlation between cloud thickness and brightness using Nimbus 4 THIR data (11.5 channel) and ATS 3 digital data. *J. Appl. Meteor.*, **13**, 402–410.

Prabhakara, C., B. J. Conrath, R. A. Hanel and E. J. Williamson, 1970: Remote sensing of atmospheric ozone using 9.6 μm band. *J. Atmos. Sci.*, **27**, 689–697.

Smith, W. L., 1968: An improved method for calculating tropospheric temperature and moisture from satellite radiometer measurements. *Mon. Wea. Rev.*, **96**, 387–396.

——, 1970: Iterative solution of the radiative transfer equation for the temperature and absorbing gas profile of an atmosphere. *Appl. Opt.*, **9**, 1993–1999.

——, H. M. Woolf and W. J. Jacob, 1970: A regression method for obtaining real time temperatures and geopotential height profiles from satellite spectrometer measurements and its application to Nimbus 3 SIRS observations. *Mon. Wea. Rev.*, **98**, 582–594.

——, P. G. Abel, H. M. Woolf, A. W. McCulloch and B. J. Johnson, 1975: The high resolution infrared radiation sounder (HIRS) experiment. *Nimbus 6 User's Guide*, Goodard Space Flight Center, Greenbelt, Md., 227 pp.

Stoffel, T. L., 1976: Radiative properties of cirrus clouds in the infrared: Application to remote sensing. Master's thesis, University of Utah, Salt Lake City, 99 pp.

Taylor, F. W., 1974: Remote temperature sounding in the presence of cloud by zenith scanning. *Appl. Opt.*, **13**, 1559–1566.